Hamburger Beiträge
zur Angewandten Mathematik

A Finite Volume Projection Method for Incompressible Flows on Triangular Grids

N. Botta and D. Hempel

submitted to Journal of Computational Physics

Reihe A

Preprint 110

September 1996

Hamburger Beiträge zur Angewandten Mathematik

Reihe A Preprints
Reihe B Berichte
Reihe C Mathematische Modelle und Simulation
Reihe D Elektrische Netzwerke und Bauelemente
Reihe E Scientific Computing

A FINITE VOLUME PROJECTION METHOD FOR INCOMPRESSIBLE FLOWS ON TRIANGULAR GRIDS

N. BOTTA AND D. HEMPEL

ABSTRACT. In this paper we present a finite volume projection method for two-dimensional incompressible flows. The unsteady Navier-Stokes equations are discretized on a triangular unstructured grid.

The velocity field is approximated by means of either piecewise constant or piecewise linear functions, the pressure field with piecewise linear functions. We require the momentum equation to be weakly satisfied on the triangles; the continuity equation $\nabla \cdot u = 0$ is enforced on the "boxes" constructed around the nodes of the grid. The convective term is approximated with a second order Godunov scheme. For the computation of the diffusive fluxes a dual grid connecting the centers of the triangles of the original grid is introduced. Gradient of pressure and divergence of the velocity field are discretized in such a way that i) the discrete gradient of the pressure vanishes if and only if the pressure is a constant function; ii) the discrete gradient and divergence are dual; iii) the discrete divergence of the approximate velocity field is zero.

The method is second order accurate on smooth flows. The Poisson problem arising from the projection step can be solved with standard iterative methods.

The numerical results confirm the accuracy of the method and indicate that no local decoupling of the pressure field occurs.

1. INTRODUCTION

In this paper we present a finite volume projection method for the numerical approximation of two-dimensional incompressible flows. We consider the unsteady Navier-Stokes equations

$$\frac{\partial u}{\partial t} = \nu \Delta u - u \cdot \nabla u - \nabla p \qquad \text{on } \mathcal{D} \times (0, T], \tag{1}$$

$$\nabla \cdot u = 0 \qquad \text{on } \mathcal{D} \times (0, T] \tag{2}$$

for the velocity u and the pressure p. Both u and p are functions of the space coordinate $x \in \mathcal{D} \cup \partial\mathcal{D}$ and of the time $t \in [0, T]$. $\mathcal{D}$ is a bounded domain of $I\!R^2$, $\partial\mathcal{D}$ is the boundary of $\mathcal{D}$ and $[0, T] \subset I\!R^+$. For suitable initial and boundary conditions we want to compute approximations to u and p on triangular unstructured grids.

We seek a numerical method which is accurate and robust both for flows at low Reynolds numbers and for inviscid flows. The aim is to provide the framework for

It is our pleasure to thank O. Friedrich for providing the codes for grid generation, flow visualization and some linear system solver.

the development of numerical methods to be used in the simulation of unsteady combustion processes in complex geometries.

The idea is to obtain the pressure by means of a discrete projection as originally proposed by Chorin [9], [10], [11]. Let u^t represent the velocity field at time t. The velocity at a later time $u^{t+\delta t}$ is obtained by integrating the acceleration (1) over the time interval $[t, t+\delta t]$.

$$u^{t+\delta t} = u^t + \int_t^{t+\delta t} (\nu \Delta u - u \cdot \nabla u)\, dt - \int_t^{t+\delta t} \nabla p \, dt. \tag{3}$$

The time integral of the pressure, in turn, is obtained by enforcing the incompressibility constraint (2) on the new velocity $u^{t+\delta t}$:

$$\nabla \cdot u^{t+\delta t} = 0 \quad \Longrightarrow \quad \int_t^{t+\delta t} \Delta p \, dt = \nabla \cdot u^t + \nabla \cdot \int_t^{t+\delta t} (\nu \Delta u - u \cdot \nabla u)\, dt. \tag{4}$$

The last equation is a Poisson problem for the average pressure over the time interval $[t, t+\delta t]$.

Projection methods based on second order Godunov schemes for the upwind discretization of the convective term have been introduced by Bell, Colella and Glaz [3] and Bell, Colella and Howell [4]. These methods provide a robust discretization of $u \cdot \nabla u$ and are well suited for the numerical computation of flows at high Reynolds numbers and for inviscid flows. They have been extended to describe variable density flows [6], three dimensional flows [5] as well as to flows with moving interfaces [18] such as those arising in the simulation of combustion processes.

Although very successful, the projection methods based on the algorithms proposed in [3] and [4] have a few shortcomings. One lies in the discretization of the pressure gradient G. In these methods the dimension of $\ker G$ is greater than one (in the continuous case $\dim \ker G = 1$). As explained in [14] a consequence of $\dim \ker G > 1$ is that the method may exhibit local grid decoupling. This results in oscillations of the pressure field. In the methods referenced above the problem is solved by introducing nonstandard discretization of the Laplace operator for the Poisson problem. As a consequence nonstandard iterative procedures have to be used to solve this problem.

In a recent work Almgren, Bell and Szymczak [1] propose an approximate projection which overcomes the problems related with local grid decoupling. The method retains the essentials of the original formulation but avoids the exact enforcement of the incompressibility condition (2): the velocity field obtained with the projection step is required to be divergence-free to second order accuracy.

All finite volume projection methods mentioned above have been designed for structured grids. Discrete projections for unstructured triangular grids have been mostly developed in the frame of finite element methods. In this context a deeper insight in the understanding of the relationship between local grid decoupling and instability has been obtained by re-formulating the governing equations as a variational problem. For the steady Stokes equations necessary and sufficient conditions for stability have been derived by Babuška and Brezzi [2], [8]. When applied to a discrete problem the Babuška-Brezzi conditions result in restrictions for the functional spaces used to approximate u and p.

The practical implication of these restrictions is that the dimension of the functional space used to approximate the velocity must be higher than the dimension of the space where a numerical approximation for the pressure is sought: on triangular elements, for instance, the standard Galerkin method with piecewise linear functions for velocity components and pressure turns out to be unstable.

Different techniques have been proposed in order to overcome the stability problem without introducing higher order interpolating functions. An extensive review of stabilized formulations for finite element methods is presented in [16].

Stabilization techniques are based either on the enrichment of the velocity space (see [14]) or on the introduction of source terms in the governing equations. These terms, in the form of some residual, are designed to limit the degrees of freedom of the pressure without introducing new unknown velocities and still preserving consistency of the numerical scheme with the governing equations.

In the development of our numerical method we have used a somewhat different approach: the method is based on the following guidelines:

1. we want to construct a second order finite volume projection method based on a triangle-centered discretization of the velocity;
2. the differential operators should be discretized in order to avoid any local grid decoupling;
3. the discrete divergence of the velocity field obtained from the projection step should be zero;
4. the linear system resulting from the discretization of the Poisson problem for the pressure should be efficiently solved with standard iterative methods;
5. we want to use at most piecewise linear ansatz functions both for the velocity and for the pressure.

We have essentially two reasons to prefer a triangle-centered discretization of the velocity field. First we want to avoid having velocity unknowns which represent both average values and boundary values. This would happen, in a node-centered formulation, at the nodes laying on the boundaries of the computational domain. A triangle-centered formulation avoids this conflict. It also allows the localization of average values of the velocity in the center of the control volumes: this choice is consistent with a second order approximation.

The second reason for choosing a triangle-centered formulation for the velocity is related with the second issue listed above. We hope to avoid local grid decoupling by discretizing the gradient of the pressure in such a way that

i) the discrete gradient of the pressure vanishes if and only if the pressure is a constant function.

This can be easily achieved if we approximate p by means of standard piecewise linear functions on the triangles and require the momentum equation to be weakly satisfied on the triangles. For this we need as many velocity unknowns as triangles and a triangle-centered discretization of the velocity is the natural choice.

In order to satisfy the requirements 3., 4. and 5. we discretize the divergence of the velocity field in such a way that

ii) the discrete gradient and divergence are dual;

iii) the discrete divergence of the approximate velocity field is zero.

A discrete divergence D that fulfills ii) and iii) can be obtained by weakly enforcing the incompressibility constraint (2) on the boxes constructed around the nodes of the grid (figure 1, left) and using piecewise constant velocities on the triangles. This leads to a discrete Laplacian which is positive definite and symmetric. Thus a standard conjugate gradients method can be used to solve the Poisson problem for the pressure.

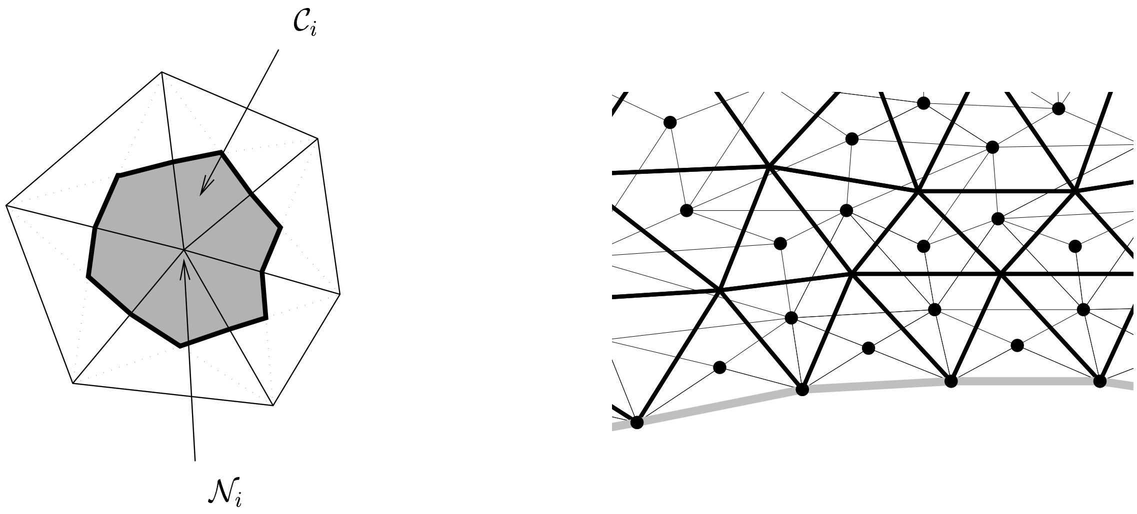

FIGURE 1. Left: construction of the box $\mathcal{C}_i$ around node $\mathcal{N}_i$. Right: primary (fat lines) and dual grid (thin lines). The dual grid is constructed by connecting the centers of the triangles and the boundary nodes of the original grid to each other.

The reason for restricting our ansatz functions to be piecewise linear is that we seek a numerical method which can be extended to the three-dimensional case with affordable memory requirements.

For the discretization of the Laplacian of the velocity a dual grid is introduced. This consists of triangles connecting the centers of the triangles and the boundary nodes of the grid (figure 1, right). The triangle-averages of the velocity are then re-interpreted as nodal values of a piecewise linear function defined on the triangles of the dual grid.

The rest of this paper is organized as follows: in section 2 we formulate the finite volume projection method by deriving it from the governing equations. We introduce a numerical approximation $(\tilde{u}, \tilde{p})$ to the true solution (u, p) of the continuous problem and we derive discrete forms of gradient and divergence for which i), ii) and iii) hold. In section 3 we discuss the approximation of the convective and of the diffusive fluxes. Section 4 deals with boundary conditions. We discuss the effect of non-homogeneous boundary conditions and propose a treatment of outflow boundaries for flows at high Reynolds numbers.

In section 5 we present numerical results for three problems. The first one is a Poiseuille flow between two flat plates. We use this problem to make a convergence study of the method. The second test case is a shear-driven cavity flow at Reynolds number 100, 1000 and 10000. For the flow at Reynolds number 1000 we compare our numerical results with those presented in [17]. The last test case is the one proposed for two-dimensional incompressible flows in the frame of the DFG Priority Research Programme "Flow Simulation on High Performance Computers". The set up consist of a circular cylinder asymmetrically placed between two flat plates. We compare the numerical results obtained in the steady (Reynolds number 20) and in the unsteady case (Reynolds number 100) with those reviewed in [15].

In the last section we draw a few conclusions and outline the work to be done.

2. Finite volume projection method

Consider the incompressible Navier-Stokes equations (1), (2) with initial and boundary conditions

$$u = b \qquad \text{on } \partial\mathcal{D} \times [0, T], \tag{5}$$

$$u = u^0 \qquad \text{on } \mathcal{D} \cup \partial\mathcal{D} \text{ at } t = 0. \tag{6}$$

We will assume that $b(x,t)$ and $u^0(x)$ satisfy the following constraints

$$\nabla \cdot u^0 = 0 \qquad \text{on } \mathcal{D}, \tag{7}$$

$$b \cdot n = u^0 \cdot n \qquad \text{on } \partial\mathcal{D} \text{ at } t \geq 0, \tag{8}$$

$$\int_{\partial\mathcal{D}} b \cdot n \, d\mathcal{S} = 0 \qquad \text{for } t \geq 0. \tag{9}$$

These assumptions seem to be reasonable in order to have a well posed problem, see the remarks at page 51–52 of [13] and the discussion presented in [7] on the role of

(8) for problems with inflow and outflow boundaries. A boundary condition for the pressure is not required.

We seek a weak formulation of equations (3) and (4). Let $\mathcal{D}$ be covered by a conformal triangulation consisting of a set of nodes $\mathcal{N} := \{\mathcal{N}_1, \dots, \mathcal{N}_N\}$ and of triangles $\mathcal{T} := \{\mathcal{T}_1, \dots, \mathcal{T}_M\}$. Let $\mathcal{C}$ be the set of the boxes constructed around the nodes of the grid: $\mathcal{C} := \{\mathcal{C}_1, \dots, \mathcal{C}_N\}$ (figure 1, left). Let $Q_\mathcal{T}$ and $Q_\mathcal{C}$ be the spaces of piecewise constant functions on the triangles and on the boxes:

$$Q_\mathcal{T} \ := \ \mathrm{span}\{\chi_{\mathcal{T}_1}, \dots, \chi_{\mathcal{T}_M}\} \qquad Q_\mathcal{C} \ := \ \mathrm{span}\{\chi_{\mathcal{C}_1}, \dots, \chi_{\mathcal{C}_N}\}$$

In the above definitions $\chi_{\mathcal{T}_j}$ and $\chi_{\mathcal{C}_i}$ are the characteristic functions of $\mathcal{T}_j$ and of $\mathcal{C}_i$, respectively. Let $t^k := t$, $t^{k+1} := t + \delta t$, $u^k := u^t$, $u^{k+1} := u^{t+\delta t}$ and

$$f \ := \ \nu \Delta u - u \cdot \nabla u.$$

We request equation (3) to be weakly satisfied on the triangles

$$|\mathcal{T}_j| \, u_j^{k+1} = |\mathcal{T}_j| \, u_j^k + \delta t \int_{\mathcal{T}_j} f^{k+1/2} \, d\mathcal{V} - \delta t \int_{\mathcal{T}_j} \nabla p^{k+1/2} \, d\mathcal{V} \qquad j = 1, \dots, M. \tag{10}$$

In the last equation u_j^k, u_j^{k+1} represent the averages of u^k, u^{k+1} on the triangle $\mathcal{T}_j$; $|\mathcal{T}_j|$ is the area of $\mathcal{T}_j$; $f^{k+1/2}$ and $p^{k+1/2}$ are the time averages of f and p over $[t^k, t^{k+1}]$.

The incompressibility constraint (4) is weakly enforced on the boxes constructed around the nodes of the grid; using Gauss theorem to transform the integral over $\mathcal{C}_i$ into an integral over the boundary $\partial\mathcal{C}_i$ one has

$$\delta t \int_{\partial\mathcal{C}_i} \nabla p^{k+1/2} \cdot n \, d\mathcal{S} = \int_{\partial\mathcal{C}_i} u^k \cdot n \, d\mathcal{S} + \delta t \int_{\partial\mathcal{C}_i} f^{k+1/2} \cdot n \, d\mathcal{S} \qquad i = 1, \dots, N. \tag{11}$$

In equation (11) n is the unit vector normal to $\partial\mathcal{C}_i$. The boundary condition for the normal derivative of the average pressure on $\partial\mathcal{D}$ is derived by multiplying equation (3) with the unit vector normal to $\partial\mathcal{D}$. Let this vector be n as well. Then

$$\delta t \nabla p^{k+1/2} \cdot n \ = \ u^k \cdot n \ + \ \delta t f^{k+1/2} \cdot n \ - \ u^{k+1} \cdot n \qquad \text{on } \partial\mathcal{D}. \tag{12}$$

Notice that the first two terms on the right hand side of the last equation need not to be computed explicitly: when (12) is integrated over $\partial\mathcal{C}_i \cap \partial\mathcal{D}$ they cancel out with the corresponding terms on the right hand side of the Poisson problem (11).

Given the averages u_j^k one is not, in general, able to compute u_j^{k+1} exactly. This is due to the fact that $f^{k+1/2}$ and, through (11), $p^{k+1/2}$ depend on the solution u. Let $\tilde{u}_j^k := u_j^k$. Let $\tilde{u}^k$, $\tilde{f}^{k+1/2}$, $\tilde{p}^{k+1/2}$ be numerical approximations to u^k, $f^{k+1/2}$ and $p^{k+1/2}$, respectively. A numerical approximation $\tilde{u}_j^{k+1}$ to the exact triangle averages

u_j^{k+1} is then obtained by means of the finite volume projection method

$$|\mathcal{T}_j|\,\tilde{u}_j^{k+1} = |\mathcal{T}_j|\,\tilde{u}_j^k + \delta t \int\limits_{\mathcal{T}_j} \tilde{f}^{k+1/2}\,d\mathcal{V} - \delta t \int\limits_{\mathcal{T}_j} \nabla\tilde{p}^{k+1/2}\,d\mathcal{V} \qquad j = 1,\dots,M, \tag{13}$$

$$\delta t \int\limits_{\partial\mathcal{C}_i} \nabla\tilde{p}^{k+1/2}\cdot n\,d\mathcal{S} = \int\limits_{\partial\mathcal{C}_i} \tilde{u}^k\cdot n\,d\mathcal{S} + \delta t \int\limits_{\partial\mathcal{C}_i} \tilde{f}^{k+1/2}\cdot n\,d\mathcal{S} \qquad i = 1,\dots,N. \tag{14}$$

Let $V := \operatorname{span}\{\varphi_1,\dots,\varphi_N\}$ where φ_i is the linear function having the value 1 at the node $\mathcal{N}_i$ and 0 in the other nodes. V is the space of the piecewise linear functions on the triangles. Let $\tilde{p} := \sum_{i=1}^N \tilde{p}_i\varphi_i \in V$ and $\tilde{u} := \sum_{j=1}^M \tilde{u}_j\chi_{\mathcal{T}_j} \in Q^2_{\mathcal{T}}$. The discrete pressure gradient G is defined as

$$G \;:\; V \ni \tilde{p} \longrightarrow G(\tilde{p}) \;:=\; \sum_{j=1}^M G_j(\tilde{p})\chi_{\mathcal{T}_j} \;\in\; Q^2_{\mathcal{T}} \tag{15}$$

$$G_j(\tilde{p}) \;:=\; \frac{1}{|\mathcal{T}_j|}\int\limits_{\mathcal{T}_j} \nabla\tilde{p}\,d\mathcal{V} \;=\; \sum_{i\in I(\mathcal{T}_j)} \tilde{p}_i\nabla\varphi_i^j. \tag{16}$$

In the above definition $I(\mathcal{T}_j)$ represents the set of indexes of the nodes belonging to the triangle $\mathcal{T}_j$ and $\nabla\varphi_i^j$ is the gradient of the i-th base function of V over the triangle $\mathcal{T}_j$. The discrete divergence is

$$D \;:\; Q^2_{\mathcal{T}} \ni \tilde{u} \longrightarrow D(\tilde{u}) \;:=\; \sum_{i=1}^N D_i(\tilde{u})\chi_{\mathcal{C}_i} \;\in\; Q_{\mathcal{C}} \tag{17}$$

$$\begin{aligned} D_i(\tilde{u}) \;:=\; \frac{1}{|\mathcal{C}_i|}\int\limits_{\partial\mathcal{C}_i\setminus\partial\mathcal{D}} \tilde{u}\cdot n\,d\mathcal{S} \;&=\; \frac{1}{|\mathcal{C}_i|}\sum_{j\in J(\mathcal{N}_i)} \tilde{u}_j\cdot \int\limits_{(\partial\mathcal{C}_i\setminus\partial\mathcal{D})\cap\mathcal{T}_j} n\,d\mathcal{S} \\ &=\; -\frac{1}{|\mathcal{C}_i|}\sum_{j\in J(\mathcal{N}_i)} |\mathcal{T}_j|\tilde{u}_j\cdot\nabla\varphi_i^j. \end{aligned} \tag{18}$$

$J(\mathcal{N}_i)$ is now the set of indexes of the triangles sharing the node $\mathcal{N}_i$. The last equality on the right hand side of (18) can be easily proved.

Let $\tilde{p}^{k+1/2} \in V$ and $\tilde{u}^k$, $\tilde{u}^{k+1}$, $\tilde{f}^{k+1/2} \in Q^2_{\mathcal{T}}$. Let $\tilde{b} \in C^0(\partial\mathcal{D}, I\!R^2)$ be an approximation to the boundary condition b. In section 4 we will give a precise definition of this approximation.
We require $\tilde{u}^k$, $\tilde{u}^{k+1}$ and $\tilde{p}^{k+1/2}$ to satisfy the boundary conditions:

$$\tilde{u}^k\cdot n \;=\; \tilde{b}^k\cdot n, \qquad \tilde{u}^{k+1}\cdot n \;=\; \tilde{b}^{k+1}\cdot n \qquad \text{on } \partial\mathcal{D}, \tag{19}$$

$$\delta t\nabla\tilde{p}^{k+1/2}\cdot n \;=\; \tilde{b}^k\cdot n \;+\; \delta t\tilde{f}^{k+1/2}\cdot n \;-\; \tilde{b}^{k+1}\cdot n \qquad \text{on } \partial\mathcal{D}. \tag{20}$$

Equations (19), (20) follow from the boundary conditions (5) and (12) for the exact solution (u, p).

Consider the Poisson problem (14). Splitting $\partial\mathcal{C}_i$ in its boundary part $\partial\mathcal{C}_i \cap \partial\mathcal{D}$ and internal part $\partial\mathcal{C}_i \setminus \partial\mathcal{D}$ this equation can be written as:

$$\begin{aligned}
& \int\limits_{\partial\mathcal{C}_i\cap\partial\mathcal{D}} \tilde{b}^k \cdot n \, d\mathcal{S} \; + \; \delta t \int\limits_{\partial\mathcal{C}_i\cap\partial\mathcal{D}} \tilde{f}^{k+1/2} \cdot n \, d\mathcal{S} \\
& - \int\limits_{\partial\mathcal{C}_i\cap\partial\mathcal{D}} \tilde{b}^{k+1} \cdot n \, d\mathcal{S} \; + \; \delta t \int\limits_{\partial\mathcal{C}_i\setminus\partial\mathcal{D}} \nabla\tilde{p}^{k+1/2} \cdot n \, d\mathcal{S} \\
= \; & \int\limits_{\partial\mathcal{C}_i\cap\partial\mathcal{D}} \tilde{b}^k \cdot n \, d\mathcal{S} \; + \int\limits_{\partial\mathcal{C}_i\setminus\partial\mathcal{D}} \tilde{u}^k \cdot n \, d\mathcal{S} \\
& + \delta t \int\limits_{\partial\mathcal{C}_i\cap\partial\mathcal{D}} \tilde{f}^{k+1/2} \cdot n \, d\mathcal{S} \; + \; \delta t \int\limits_{\partial\mathcal{C}_i\setminus\partial\mathcal{D}} \tilde{f}^{k+1/2} \cdot n \, d\mathcal{S},
\end{aligned} \tag{21}$$

for $i = 1, \ldots, N$. In the right hand side of the above equation (19) has been used to express the integral of $\tilde{u}^k \cdot n$ on $\partial\mathcal{D}$. The first three terms are obtained by expressing $\nabla\tilde{p}^{k+1/2} \cdot n$ on $\partial\mathcal{D}$ by means of the boundary condition (20). As in the continuous case $\tilde{u}^k \cdot n$ and $\tilde{f}^{k+1/2} \cdot n$ need not to be evaluated on $\partial\mathcal{D}$: the first and the second term of (22) cancel out with the fifth and with the seventh integral.

Using (15) the discrete projection (13) can be written, after division through $|\mathcal{T}_j|$, as

$$\tilde{u}^{k+1} = \tilde{u}^k + \delta t \tilde{f}^{k+1/2} - \delta t G(\tilde{p}^{k+1/2}). \tag{22}$$

Let $I_\mathcal{C}$ be the linear operator:

$$I_\mathcal{C} \; : \; Q_\mathcal{C} \; \ni \; q := \sum_{i=1}^{N} q_i \chi_{\mathcal{C}_i} \; \longrightarrow \; I_\mathcal{C}(q) := \sum_{i=1}^{N} |\mathcal{C}_i| q_i \chi_{\mathcal{C}_i} \; \in \; Q_\mathcal{C}. \tag{23}$$

Using the above definition and equations (15)–(18) The Poisson problem (22) can be written as

$$\delta t I_\mathcal{C}(D(G(\tilde{p}^{k+1/2}))) = I_\mathcal{C}\left(D(\tilde{u}^k) + \delta t D(\tilde{f}^{k+1/2}) + D^b(\tilde{b}^{k+1})\right). \tag{24}$$

In equation (24) D^b is the linear operator

$$\begin{aligned}
D^b \; & : \; C^0(\partial\mathcal{D}, I\!R^2) \; \ni \; \tilde{u} \; \longrightarrow \; D^b(\tilde{u}) \; := \; \sum_{i=1}^{N} D_i^b(\tilde{u}) \chi_{\mathcal{C}_i} \; \in \; Q_\mathcal{C} \\
D_i^b(\tilde{u}) \; & := \; \frac{1}{|\mathcal{C}_i|} \int\limits_{\partial\mathcal{C}_i\cap\partial\mathcal{D}} \tilde{u} \cdot n \, d\mathcal{S}
\end{aligned}$$

$D^b(\tilde{b}^{k+1})$ accounts for the third integral of equation (22) and represents the effect of mass flux through the boundary of $\mathcal{D}$.

$Lp := D \circ G$ is the discrete Laplacian for the pressure. Using the definitions of G and of D given above one can easily verify that $Lp : V \longrightarrow Q_{\mathcal{C}}$ has a compact stencil; this consist of all nodes which are connected to $\mathcal{N}_i$ by means of one segment. A straightforward algebra shows that $I_{\mathcal{C}} \circ Lp$ is nothing but the integral of the Laplace operator which is obtained with the standard piecewise linear Galerkin approximation in the frame of finite elements methods. Its associated matrix is symmetric and positive definite. Thus a standard iterative method can be used to compute the pressure as a solution of the Poisson problem (24). In our computations we have used the method of conjugate gradients.

The transformations G and D have been defined according to equations (13) and (14); they are linear transformations and $\dim V = \dim Q_{\mathcal{C}} = N$, $\dim Q_{\mathcal{T}} = M$.
In the rest of this section we show that for the discrete gradient and divergence the statements i), ii) and iii) made in the introduction hold. Then, in the next section, we introduce a time discretization and show how to compute $\tilde{f}^{k+1/2}$.

Remark 1. Let $\tilde{p} := \sum_{i=1}^{N} \tilde{p}_i \varphi_i \in V$. Then $G(\tilde{p}) = 0$ if and only if $\tilde{p}$ is a constant function.

Let $\tilde{p} = c$ i.e. $\tilde{p}_i = c,\ i = 1, \ldots, N$. From (16) follows

$$G_j(\tilde{p}) \;=\; c\,|\mathcal{T}_j| \sum_{i \in I(\mathcal{T}_j)} \nabla \varphi_i^j \;=\; 0 \qquad j = 1, \ldots, M.$$

Conversely assume that $\tilde{p}$ is not constant. Then there is at least one triangle, say $\mathcal{T}_j$, such that $\tilde{p}|_{\mathcal{T}_j}$ is not constant. Thus $G_j(\tilde{p}) \neq 0$ and $G(\tilde{p}) \neq 0$.

Remark 2. Let G, D and $I_{\mathcal{C}}$ be the $2M \times N$, $N \times 2M$ and $N \times N$ matrices associated to the linear transformations (15), (17) and (23) (for $\{\chi_{\mathcal{T}_1}, \ldots, \chi_{\mathcal{T}_M}\}$, $\{\chi_{\mathcal{C}_1}, \ldots, \chi_{\mathcal{C}_N}\}$ and $\{\varphi_1, \ldots, \varphi_N\}$ bases of $Q_{\mathcal{T}}$, $Q_{\mathcal{C}}$ and V respectively). Let $I_{\mathcal{T}}$ be the linear operator:

$$I_{\mathcal{T}} \;:\; Q_{\mathcal{T}}^2 \;\ni\; q := \sum_{j=1}^{M} q_j \chi_{\mathcal{T}_j} \;\longrightarrow\; I_{\mathcal{T}}(q) := \sum_{j=1}^{M} |\mathcal{T}_j| q_j \chi_{\mathcal{T}_j} \;\in\; Q_{\mathcal{T}}^2.$$

and $I_{\mathcal{T}}$ its $2M \times 2M$ associated matrix (for $\{\chi_{\mathcal{T}_1}, \ldots, \chi_{\mathcal{T}_M}\}$ basis of $Q_{\mathcal{T}}$). Then $(I_{\mathcal{C}} D)_{ij} \;=\; -\,(I_{\mathcal{T}} G)_{ji}$.

Consider the element $(I_{\mathcal{T}} G)_{ji}$ of the matrix $I_{\mathcal{T}} G$. One has

$$(I_{\mathcal{T}} G)_{ji} \;= \begin{cases} |\mathcal{T}_j|\, \nabla \varphi_i^j & \text{if } i \in I(\mathcal{T}_j) \\ 0 & \text{otherwise.} \end{cases}$$

On the other hand

$$(I_{\mathcal{C}}D)_{ij} \;=\; \begin{cases} \displaystyle\int\limits_{\partial\mathcal{C}_i\cap\mathcal{T}_j} n\, d\mathcal{S} \;=\; -\,|\mathcal{T}_j|\,\nabla\varphi_i^j & \text{if } j \in J(\mathcal{N}_i) \\ \qquad\qquad 0 & \text{otherwise.} \end{cases}$$

Since $i \in I(\mathcal{T}_j) \iff j \in J(\mathcal{N}_i)$ one has $(I_{\mathcal{C}}D)_{ij} \;=\; -\,(I_{\mathcal{T}}G)_{ji}$ and the discrete divergence and gradient are dual.

Remark 3. Consider the piecewise contant approximation $\tilde{u}^{k+1}$ obtained with the finite volume projection method (22), (24). One has

$$\int\limits_{\partial\mathcal{C}_i} \tilde{u}^{k+1}\!\cdot n\, d\mathcal{S} \;=\; 0 \qquad i = 1, \ldots, N.$$

This can be easily seen by expressing $\tilde{u}^{k+1}$ in the above equations with (22), splitting the integrals over $\partial\mathcal{C}_i$ in boundary and internal integrals and using (24) and the boundary condition (20).

3. Computation of the fluxes, algorithm

As seen in the previous section $\tilde{f}^{k+1/2} \in Q^2_{\mathcal{T}}$ is a piecewise constant approximation to the time average $f^{k+1/2}$ of the flux function f over $[t^k, t^{k+1}]$

$$\tilde{f}^{k+1/2} \approx f^{k+1/2} := \frac{1}{\delta t}\int\limits_{t^k}^{t^{k+1}} f\, dt = \frac{1}{\delta t}\int\limits_{t^k}^{t^{k+1}} \nu\Delta u\, dt - \frac{1}{\delta t}\int\limits_{t^k}^{t^{k+1}} u\cdot\nabla u\, dt$$

Let $\tilde{f}^{k+1/2} = \tilde{fd}^{k+1/2} + \tilde{fc}^{k+1/2}$:

$$\tilde{fd}^{k+1/2} \;:=\; \sum_{j=1}^{M} \tilde{fd}_j^{k+1/2}\chi_{\mathcal{T}_j} \qquad \tilde{fc}^{k+1/2} \;:=\; \sum_{j=1}^{M} \tilde{fc}_j^{k+1/2}\chi_{\mathcal{T}_j} \tag{25}$$

$\tilde{fd}^{k+1/2} \in Q^2_{\mathcal{T}}$ and $\tilde{fc}^{k+1/2} \in Q^2_{\mathcal{T}}$ are piecewise constant approximations to the time averages of the viscous and of the convective fluxes, respectively.

Let us focus the attention on $\tilde{fd}^{k+1/2}$. Let $\mathcal{N}^b \subset \mathcal{N}$ be the set of nodes laying on $\partial\mathcal{D}$ and $N^b := \#\mathcal{N}^b$. Let $\mathcal{D}$ be covered by a dual grid consisting of a set of nodes $\mathcal{N}' := \{\mathcal{N}'_1, \ldots, \mathcal{N}'_{N'}\}$ and of a set of triangles $\mathcal{T}' := \{\mathcal{T}'_1, \ldots, \mathcal{T}'_{M'}\}$. The nodes of the dual grid are placed in the centers of the triangles of the original grid and on the nodes of $\mathcal{N}^b$ (figure 1, right): thus $N' = M + N^b$.

Let V' be the space of the piecewise linear functions defined on the triangles of the dual grid: $V' := \text{span}\{{\varphi'}_1, \ldots, {\varphi'}_{N'}\}$. ${\varphi'}_i$ is the linear function having the value

1 in $\mathcal{N}'_i$ and 0 in the other dual nodes. Let $\tilde{u} := \sum_{i=1}^{N'} \tilde{u}_i {\varphi'}_i \in {V'}^2$. We define the discrete Laplacian of the velocity Lu as

$$Lu \ : \ {V'}^2 \ni \tilde{u} \longrightarrow Lu(\tilde{u}) := \sum_{j=1}^{M} Lu_j(\tilde{u})\chi_{\mathcal{T}_j} \in Q_{\mathcal{T}}^2$$

$$\begin{aligned} Lu_j(\tilde{u}) &:= \frac{1}{|\mathcal{T}_j|}\int\limits_{\partial\mathcal{T}_j} \nabla\tilde{u}^k \cdot n \, d\mathcal{S}. = \frac{1}{|\mathcal{T}_j|}\sum_{l=1}^{3}\int\limits_{\partial\mathcal{T}_{j,l}} \nabla\tilde{u}^k \cdot n \, d\mathcal{S} \\ &= \frac{1}{|\mathcal{T}_j|}\sum_{l=1}^{3}\sum_{m\in J'(j,l)} \nabla\tilde{u}^k|_{\mathcal{T}'_m} \cdot \int\limits_{\partial\mathcal{T}_{j,l}\cap\mathcal{T}'_m} n \, d\mathcal{S} \end{aligned}$$

In the above equations $\partial\mathcal{T}_{j,l}$ is the l-th side of the triangle $\mathcal{T}_j$; $J'(j,l)$ is the set of indexes of the dual triangles covering the l-th side of $\mathcal{T}_j$ (figure 2) and $\nabla\tilde{u}^k|_{\mathcal{T}'_m}$ is the value of the gradient of $\tilde{u}^k$ on the dual triangle $\mathcal{T}'_m$. With the triangle averages $\tilde{u}_j^k$,

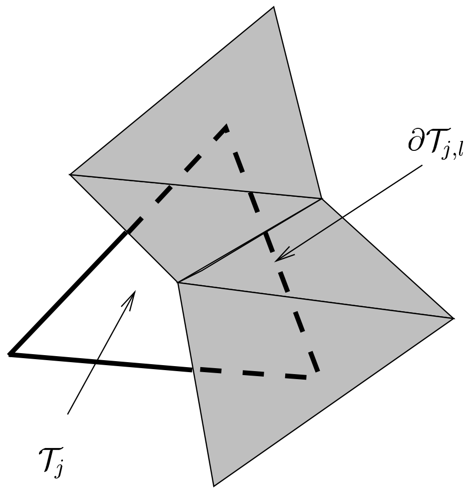

FIGURE 2. The dual triangles covering the l-th side of the j-th triangle (left).

$\tilde{u}_j^{k+1}$ $j = 1, \ldots, M$ and the approximations $\tilde{b}^k$, $\tilde{b}^{k+1} \in C^0(\partial\mathcal{D}, I\!R^2)$ of the boundary conditions $b(x,t^k)$, $b(x,t^{k+1})$ to be defined in the next section we construct the piecewise linear function $\tilde{u}^k \in {V'}^2$

$$\tilde{u}^k := \sum_{i=1}^{N'} \tilde{u}_i^k {\varphi'}_i, \quad \tilde{u}_i^k := \begin{cases} \tilde{u}_l^k & \text{if } \mathcal{N}'_i \text{ corresponds to the triangle } \mathcal{T}_l \in \mathcal{T} \\ \tilde{b}_m^k & \text{if } \mathcal{N}'_i \text{ corresponds to the node } \mathcal{N}_m \in \mathcal{N}^b \end{cases} \tag{26}$$

and similarly for $\tilde{u}^{k+1} \in V'^2$. In the above definition (and in the rest of this section) we abuse the symbols $\tilde{u}^k$, $\tilde{u}^{k+1}$: they represent now piecewise linear functions on the dual grid. We define the viscous fluxes $\tilde{fd}^{k+1/2}$ as:

$$\tilde{fd}^{k+1/2} := \frac{\nu}{2}\left(Lu(\tilde{u}^k) + Lu(\tilde{u}^{k+1})\right). \tag{27}$$

Let us turn the attention to the convective fluxes $\tilde{fc}^{k+1/2}$. Again we use a sloppy notation and define, on each triangle of the original grid, the piecewise linear reconstruction

$$\tilde{u}_j^{k+1/2}(x) := \tilde{u}_j^k + (\tilde{u}_t)_j^k \frac{\delta t}{2} + (\nabla\tilde{u})_j^k \cdot (x - x_j) \qquad j = 1, \dots, M. \tag{28}$$

In equation (28) $(\tilde{u}_t)_j^k$ and $(\nabla\tilde{u})_j^k$ are approximations to the averages of $\partial u/\partial t$, ∇u over the triangle $\mathcal{T}_j$ and x_j is the center of the triangle $\mathcal{T}_j$. The approximations $(\tilde{u}_t)_j^k$, $(\nabla\tilde{u})_j^k$ will be defined at the end of this section.

Using $\tilde{u}_j^{k+1/2}(x)$ we construct $\tilde{fc}_j^{k+1/2}$ with the following upwind rule:

$$\tilde{fc}_j^{k+1/2} := \frac{1}{|\mathcal{T}_j|}\sum_{l=1}^{3} |\partial\mathcal{T}_{j,l}|\tilde{fc}_{j,l}^{k+1/2} \tag{29}$$

$$\tilde{fc}_{j,l}^{k+1/2} := \left\{ \begin{array}{ll} \left\{ \begin{array}{ll} \tilde{u}_j^{k+1/2}(x_l)\tilde{v} & \text{if } \tilde{v} > 0 \\ \tilde{u}_m^{k+1/2}(x_l)\tilde{v} & \text{if } \tilde{v} \le 0 \end{array} \right. & \text{if } \partial\mathcal{T}_{j,l} \notin \partial\mathcal{D} \\ \left\{ \begin{array}{ll} \tilde{u}_j^{k+1/2}(x_l)(\tilde{u}_j^{k+1/2}(x_l)\cdot n) & \text{if } \tilde{v} > 0 \\ \tilde{b}^{k+1/2}(x_l)\tilde{v} & \text{if } \tilde{v} \le 0 \end{array} \right. & \text{if } \partial\mathcal{T}_{j,l} \in \partial\mathcal{D} \end{array} \right. \tag{30}$$

In (30) $\partial\mathcal{T}_{j,l}$ is the l-th side of the triangle $\mathcal{T}_j$ and $|\partial\mathcal{T}_{j,l}|$ its length; m is the index of the triangle of $\mathcal{T}$ sharing $\partial\mathcal{T}_{j,l}$ with $\mathcal{T}_j$ (i.e. $\partial\mathcal{T}_{j,l} = \mathcal{T}_j \cap \mathcal{T}_m$). n is the unit vector normal to $\partial\mathcal{T}_{j,l}$ oriented outwards of $\mathcal{T}_j$. $\tilde{b}^{k+1/2} \in C^0(\partial\mathcal{D}, I\!R^2)$ is again an approximation to $b(x, t^k + \delta t/2)$ to be defined in the next section. The velocity $\tilde{v}$ is

$$\tilde{v} := \left\{ \begin{array}{ll} (\tilde{u}_j^{k+1/2}(x_l) + \tilde{u}_m^{k+1/2}(x_l))\cdot n/2 & \text{if } \partial\mathcal{T}_{j,l} \notin \partial\mathcal{D} \\ \tilde{b}^{k+1/2}(x_l)\cdot n & \text{if } \partial\mathcal{T}_{j,l} \in \partial\mathcal{D} \end{array} \right. \tag{31}$$

To apply the upwind rule defined above we still have to define, on each triangle, the piecewise linear function $\tilde{u}_j^{k+1/2}(x)$. Consider the acceleration $(\tilde{u}_t)_j^k$. This is computed in a predictor stage as follows:

$$(\tilde{u}_t)_j^k := Lu_j(\tilde{u}^k) + \tilde{fc}_j^k - G_j(\tilde{p}^{k-1/2}) \tag{32}$$

In (32) $\tilde{fc}_j^k$ is computed according to (28)–(31) with $\delta t := 0$ in equation (28). Consider now the gradient $(\nabla\tilde{u})_j^k$. This is:

$$(\nabla\tilde{u})_j^k := \frac{1}{3}\sum_{i\in I(\mathcal{T}_j)} [\nabla\tilde{u}]_i^k$$

The nodal gradient $[\nabla\tilde{u}]_i^k$ is defined as the average gradient of $\tilde{u}^k \in Q_{\mathcal{T}}^2$ on the box $\mathcal{C}_i$. For an internal box, for instance

$$[\nabla\tilde{u}]_i^k := \frac{1}{|\mathcal{C}_i|}\sum_{j\in J(\mathcal{N}_i)} \tilde{u}_j^k \cdot \int_{\partial\mathcal{C}_i\cap\mathcal{T}_j} n\, d\mathcal{S}.$$

In all our computations we have used unlimited gradients.

With $\tilde{f}^{k+1/2}$ defined through (25), (27) and (29) the finite volume projection method (22), (24) reads

$$\begin{aligned} \tilde{u}^{k+1} &= \tilde{u}^k + \frac{\delta t}{2}\nu\left(Lu(\tilde{u}^k) + Lu(\tilde{u}^{k+1})\right) \\ &+ \delta t\tilde{fc}^{k+1/2} - \delta t G(\tilde{p}^{k+1/2}), \end{aligned} \tag{33}$$

$$\begin{aligned} \delta t I_{\mathcal{C}}(Lp(\tilde{p}^{k+1/2})) &= I_{\mathcal{C}}\Bigg(D(\tilde{u}^k) + \frac{\delta t}{2}\nu D\left(Lu(\tilde{u}^k) + Lu(\tilde{u}^{k+1})\right) \\ &+ \delta t D(\tilde{fc}^{k+1/2}) + D^b(\tilde{b}^{k+1})\Bigg). \end{aligned} \tag{34}$$

Equations (33), (34) are a Crank-Nicholson type implicit iteration for the unknowns $(\tilde{u}_j^{k+1}, \tilde{p}_i^{k+1/2})$, $j = 1, \ldots, M$, $i = 1, \ldots, N$. This is the same iteration analyzed by Bell, Colella and Glaz and has been treated as explained in [3].

In the numerical computation of stationary solutions one can replace this time approximation with an explicit forward Euler scheme. This is easily obtained by replacing equation (27) with

$$\tilde{fd}^{k+1/2} := \nu\, Lu(\tilde{u}^k).$$

and setting $(\tilde{u}_t)_j^k := 0$ in (28). In this case, of course, no predictor step is needed.

As final remark we would like to stress the meaning of the symbol $\tilde{u}^k$ in (33) and (34). As argument of Lu, $\tilde{u}^k$ represents a piecewise linear functions in V'^2. In the other expressions $\tilde{u}^k$ represents a piecewise constant function in $Q_{\mathcal{T}}^2$. The same is true for $\tilde{u}^{k+1}$. In fact one can think of the unknowns $\tilde{u}_j^{k+1}$, $j = 1, \ldots, M$ as the coordinates of $\tilde{u}^{k+1} \in Q_{\mathcal{T}}^2$ or as the coordinate of $\tilde{u}^{k+1} \in V'^2$.

4. Initial and boundary conditions

In this section we define the piecewise linear functions $\tilde{b}^{k+1}$, $\tilde{b}^k$ and $\tilde{b}^{k+1/2}$ appearing in the projection step, in the construction of the viscous fluxes and in the upwind rule (30).

Consider $\tilde{b}^{k+1}$ first. Let $V^b := \mathrm{span}\{\varphi_1^b, \dots, \varphi_N^b\}$ be the space of piecewise linear functions on $\partial\mathcal{D}$. Let $\tilde{b}^{k+1} := \sum_{i=1}^{N^b} \tilde{b}_i^{k+1}\varphi_i^b \in V^b \times V^b$ and $\tilde{c}^{k+1} := \sum_{i=1}^{N^b} \tilde{c}_i^{k+1}\varphi_i^b \in V^b \times V^b$. Let $\tilde{c}^{k+1}$ be defined by means of the boundary condition (5) as follows

$$\tilde{c}_i^{k+1} := b(x_i, t^{k+1}).$$

In this equation x_i is the coordinate of the node $\mathcal{N}_i \in \partial\mathcal{D}$. Let $\tilde{b}^{k+1} := \tilde{c}^{k+1}$ and consider the piecewise constant function $D^b(\tilde{b}^{k+1}) \in Q_{\mathcal{C}}$. Notice that $D^b(\tilde{b}^{k+1})$ can be different from zero only on those boxes whose boundary lies on portions of $\partial\mathcal{D}$ through which a mass flux takes place. The operator D^b defines in which weak sense the boundary condition b must satisfy the constraint (9). As seen in remark 1 the gradient of the pressure $G(\tilde{p})$ is equal to zero if $\tilde{p} \in V$ is a constant function. Therefore $\tilde{p} = 1 \in \ker G$. From the definition of D and Lp it is easy to see that $\tilde{p} = 1 \in \ker Lp$ as well. Let $R := \sum_{i=1}^N R_i\chi_{\mathcal{C}_i} \in Q_{\mathcal{C}}$. Because of the orthogonality of $\ker Lp$ and $\mathrm{im} Lp$ one must have $\sum_{i=1}^N R_i = 0$ for R to belong to $\mathrm{im} Lp$. Therefore the boundary condition $\tilde{b}$ must be chosen in such a way that

$$\sum_{i=1}^N |\mathcal{C}_i| \left(D_i(\tilde{u}^k) + \delta t D_i(\tilde{f}^{k+1/2}) + D_i(\tilde{b}^{k+1}) \right) \;=\; \sum_{i=1}^N |\mathcal{C}_i|\, D_i(\tilde{b}^{k+1}) \;=\; 0.$$

for the Poisson problem (34) to have a solution. The above condition can be easily satisfied if we define $\tilde{b}^{k+1}$ in the following way

$$\tilde{b}_i^{k+1} := \begin{cases} \tilde{c}_i^{k+1} & \text{if } \mathcal{N}_i \in \partial\mathcal{D} \setminus \partial\mathcal{D}_{out} \\ \alpha\tilde{c}_i^{k+1} & \text{if } \mathcal{N}_i \in \partial\mathcal{D}_{out} \end{cases} \tag{35}$$

In the above definition $\partial\mathcal{D}_{out}$ is the portion of $\partial\mathcal{D}$ on which an outflow takes place. The number α is computed with the inflow and outflow fluxes

$$\alpha := -\int_{\partial\mathcal{D}\setminus\partial\mathcal{D}_{out}} \tilde{c}^{k+1}\cdot n \, d\mathcal{S} \Bigg/ \int_{\partial\mathcal{D}_{out}} \tilde{c}^{k+1}\cdot n \, d\mathcal{S}\,. \tag{36}$$

the approximations $\tilde{b}^k$ and $\tilde{b}^{k+1/2}$ are defined in a similar way.

Remark 4. The definition of $\tilde{b}^{k+1}$, $\tilde{b}^k$ and $\tilde{b}^{k+1/2}$ given above makes sense as far as one knows that a given portion of $\partial\mathcal{D}$ is an outflow boundary and one can prescribe, on such portion of $\partial\mathcal{D}$, a velocity profile. In many problems these assumption are not reasonable. As an example consider the unsteady flow past a cylinder computed in section 5.

If the right end of the channel is a computational boundary then the velocity profile on the outflow section will be essentially dictated by the solution inside $\mathcal{D}$. In these cases both the magnitude and the direction of the flow on $\partial\mathcal{D}$ are, in general, unknown (for instance one may have reversed flow due to vortex shedding from the cylinder). We treat such cases as follows. First we construct a velocity profile on $\partial\mathcal{D}$ by extrapolating the velocity from inside $\mathcal{D}$. If this velocity profile is such that the flow is reversed on a portion of $\partial\mathcal{D}$ we stop the computation. Otherwise the rule (35),(36) is applied as for the case of pure Dirichlet boundary condition.

5. Numerical results

The first example is a Poiseuille flow. We have used this problem to make a convergence study of the method. Computations have been performed on a unit square for four different grids. We have used a first order forward Euler time discretization. Each computation was run until a numerical steady state was reached. In each projection step the residual of the Poisson equation was driven down to 10^{-3}.

Table 1 shows the results of the convergence study both for the Stokes equations and for the Navier-Stokes equations with Reynolds number 1 (constructed with the height of the channel and with the maximum value of the velocity imposed at the inflow) The error in the velocity components was estimated in the L_1-norm (E_1) and in the maximum norm (E_∞). The experiments indicate quadratic convergence in the L_1-norm and linear convergence in the maximum norm. For the third computation represented in table 1 ($h = 1/32$) the dual grid and the contour lines of the horizontal component of the velocity are shown in figure 3.

h	g	Stokes				Navier-Stokes			
		E_1	rate	E_∞	rate	E_1	rate	E_∞	rate
1/8	u	4.09	1.66	22.8	0.88	4.13	1.63	22.7	0.87
	v	3.76	1.76	24.3	1.17	3.94	1.77	24.4	1.16
1/16	u	1.29	1.86	12.4	0.97	1.33	1.78	12.4	0.97
	v	1.11	1.83	10.8	0.75	1.15	1.77	10.9	0.76
1/32	u	.356	1.98	6.33	0.98	.386	1.92	6.33	0.98
	v	.312	2.02	6.44	1.10	.336	1.93	6.44	1.10
1/64	u	.090		3.21		.102		3.21	
	v	.077		3.00		.088		3.00	

Table 1. Convergence study for a Poiseuille flow on a unit square.

The second example is a shear-driven cavity flow. A numerical solution has been computed for Reynolds number 100, 1000 and 10000. The Reynolds number are constructed with the length of the side of the cavity and with the velocity of the top wall. In the first two cases a numerical steady state was obtained. For the flow at Reynolds number 10000 we found a periodic solution with a low amplitude high

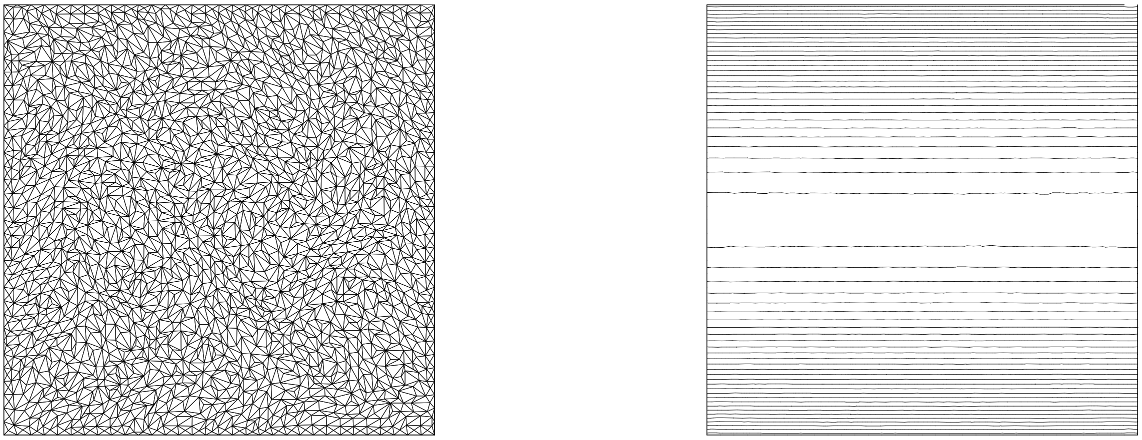

FIGURE 3. Poiseuille flow in a unit square: dual grid (4222 triangles 2176 nodes, $h = 1/32$) (left) and x-component of the velocity (right).

frequency oscillation. The computations have been performed on the same grid of 32768 triangles and 16577 nodes with a first order forward Euler time discretization. The grid has been constructed by regularly cutting a 128×128 cartesian grid. In each projection step the square of the residual of the Poisson equation was decreased of one order of magnitude.

Both grid and Reynolds numbers have been chosen in order to compare the numerical results with those reported in [17]. Figures 5 to 7 show pressure (left) and vorticity (right) contour lines. For the vorticity 17 contour lines on the interval $[-3, 5]$ have been drawn with step 0.5. In the pressure plots 90 regularly spaced contour lines have been shown between the minimal and maximal values. The results shown in these figures are in good qualitative agreement with those presented in [17] at page 404.

Let us focus the attention on the case at Reynolds number 1000 (figure 6). The diagram on the left of figure 4 shows the values of the x-component of the velocity along the vertical line through the geometric center of the cavity. The diagram on the right shows a cut of the y-component along the horizontal line through the geometric center of the cavity. The solid lines represent the numerical solution obtained with the present method. The dots represent the values reported in [17] (pag. 398 and 399).

For the flow at Reynolds number 1000 we have made two other computations. One on a grid consisting of 8192 triangles and 4193 nodes and one on a grid of 2048 triangles and 1073 nodes. In table 2 we show the value of the x-component of the velocity at the point $x = 0.5$, $y = 0.1016$ on the different grids. At this point a value of the x-component of the velocity of -0.29730 is reported in [17]. This was computed on a grid of 129×129 nodes.

FIGURE 4. Shear-driven cavity flow at Re = 1000: x-component (y-component) of the velocity along the vertical (horizontal) line through the geometric center of the cavity. Solid line: present computation; dots: results from [17].

grid	$u(0.5, 0.1016)$
2048 triangles, 1073 nodes ($h = 1/32$)	-0.2721
8192 triangles, 4193 nodes ($h = 1/64$)	-0.2932
32768 triangles, 16577 nodes ($h = 1/128$)	-0.2986

TABLE 2. Values of the x-component of the velocity at the point $x = 0.5$, $y = 0.1016$ on different grids.

It is worth mentioning that the quality of the results shown in figure 4 and in table 2 depends quite sensitively on the algorithm used in the computation of the gradients in equation 28. We have tried for instance to compute $(\nabla \tilde{u})_j^k$ by means of the arithmetic average of the gradients computed on the triangles of the dual grid sharing the node corresponding to the triangle $\mathcal{T}_j$. Although the numerical results on the fine grid were almost the same, the experiments on the rougher grids clearly indicated a more dissipative scheme.

In figure 8 we show, for the flow at Reynolds number 1000, the history of the L_2-norm of the velocity residuum versus the number of iterations for the different grids. The computational cost of a single iteration on the finest grid (25 conjugate gradients sub-iterations per iteration) was of about 5.5 seconds on a Sun SPARC station with a 50 MHz TI, TMS390Z50 processor.

The last numerical results that we want to present are those obtained for the test cases “2D-1” and “2D-2” defined for the DFG Priority Research Programme “Flow Simulation on High Performance Computers”. A complete description of these problems together with a review of the numerical results presented by 17 contributors can be found in [15]. In both cases the geometry is the same: a circular cylinder asymmetrically placed between two flat plates. The Reynolds number is 20 for the case “2D-1” and 100 for the case “2D-2”. In the first case a steady flow sets on. The flow at Reynolds number 100 is periodic. In figure 9 we show the grid used in

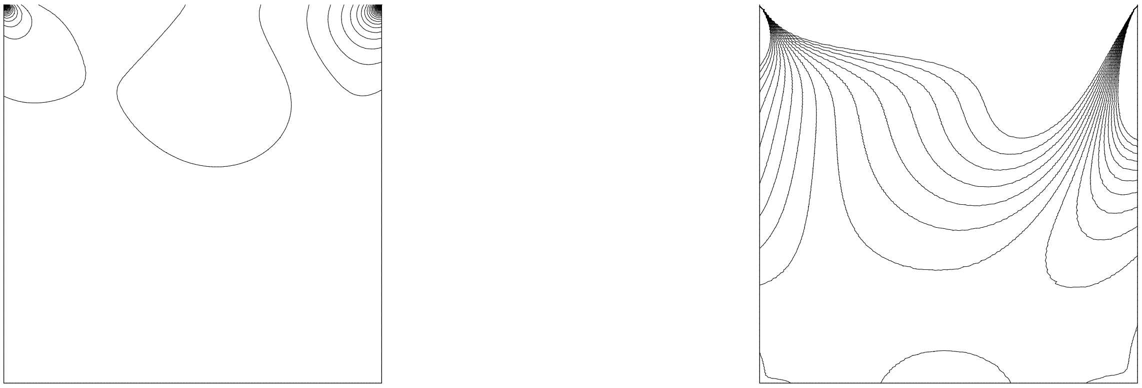

FIGURE 5. Shear-driven cavity flow at Re $=100$: pressure (left) and vorticity (right). Pressure in $[-4.21, 5.28]$.

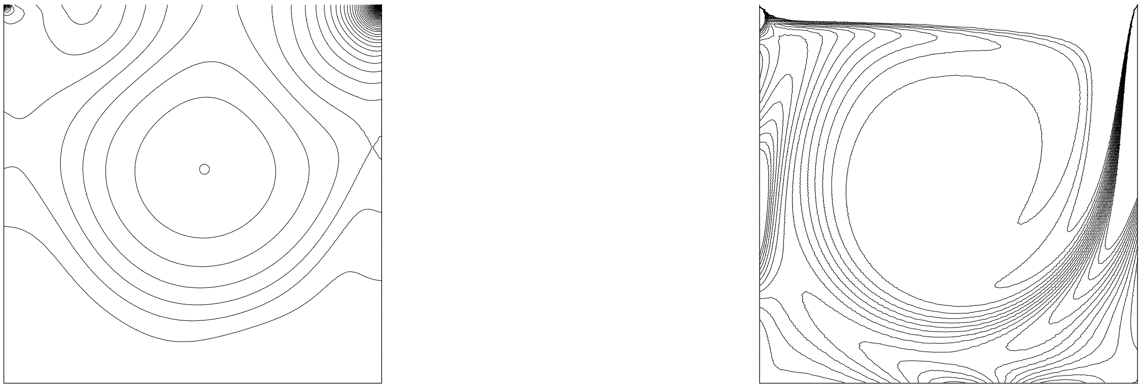

FIGURE 6. Shear-driven cavity flow at Re $=1000$: pressure (left) and vorticity (right). Pressure in $[-0.31, 1.25]$.

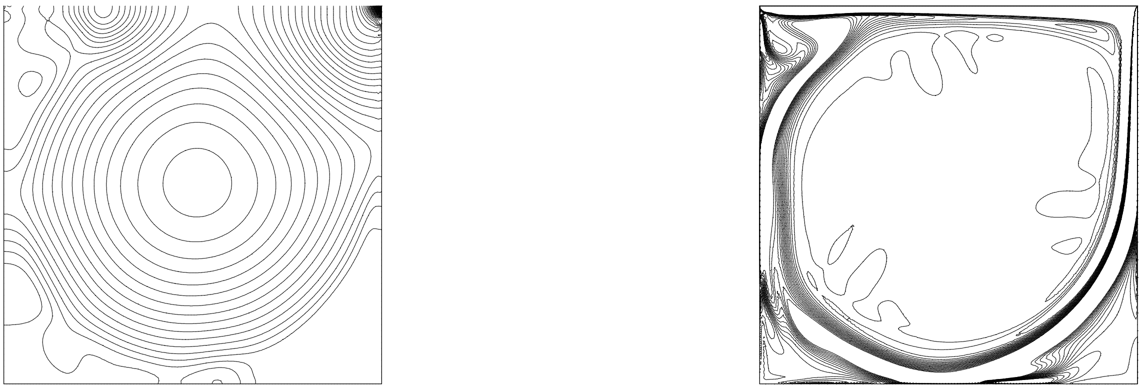

FIGURE 7. Shear-driven cavity flow at Re $=10000$: pressure (left) and vorticity (right). Pressure in $[-0.07, 0.64]$.

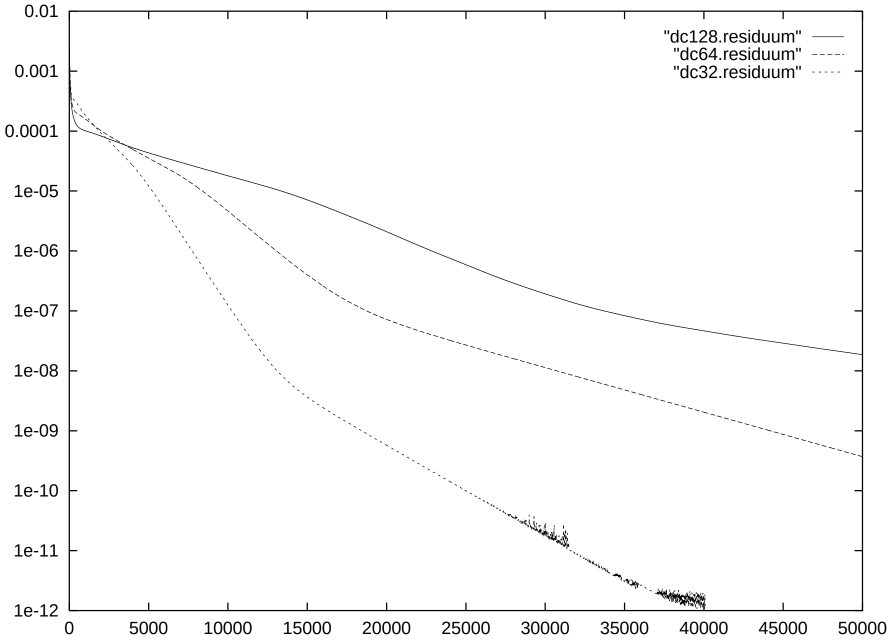

FIGURE 8. Shear-driven cavity flow at Re = 1000: residuum versus number of iterations for different grids.

both computations. It has been generated with the method described in [12]. The surface of the cylinder is covered with 128 triangles. These are equally spaced and have equal sides. The left end of the gap between the two flat plates (inflow region) is discretized with 16 triangles. The outflow is covered with 8 triangles. 80 triangles are distributed on each surface of the flat plates.

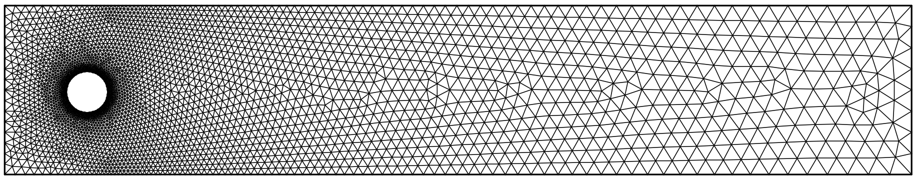

FIGURE 9. Test cases 2D-1 and 2D-2: grid; 7502 triangles and 3751 nodes.

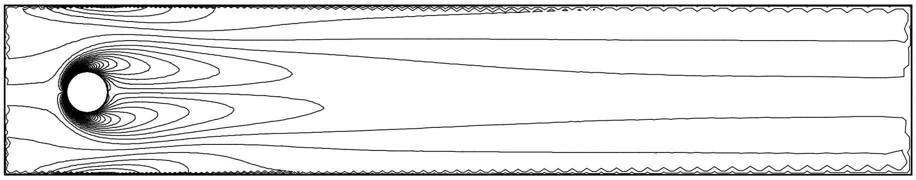

FIGURE 10. Test case 2D-1, Re = 20: vorticity contour lines.

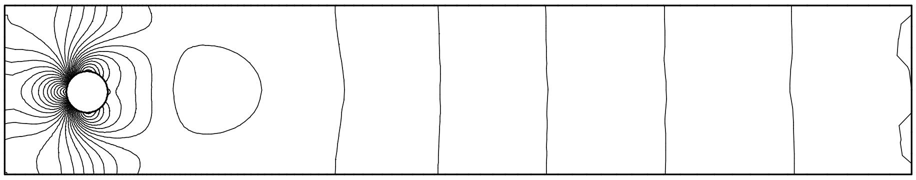

FIGURE 11. Test case 2D-1, Re = 20: pressure contour lines.

In figures 10 and 11 we show the countour lines of vorticity and pressure obtained for the flow at Reynolds number 20 at the numerical steady state. For this computation we have used the second order Crank-Nicholson type time discretization (33), (34). In each projection step the square of the residual of the Poisson equation was decreased of one order of magnitude. At the steady state the maximum absolute value of the divergence is about 10^{-9}. The wiggles in the contour lines of the vorticity in the vicinity of the boundary are due to the fact that we have not computed the vorticity at boundary points (these values were set to zero).

For this test case four quantities were to be computed: the lift coefficient C_L, the drag coefficient C_D, the pressure difference between the stagnation point in front of the cylinder and the one in the rear ΔP and the length of the recirculation area L_a. These quantities are reported in table 3. In the same table two reference values are provided. The first one (reference 1) has been obtained by averaging the results obtained by authors who have performed computations with a number of unknowns between 13299 and 22212 (in our computation we had $3751 + 2 \times 7502 = 18755$ unknowns). The second reference value is the range where the exact solution is to be expected, see [15].

	present	reference 1	reference 2
C_L	0.0113	0.0084	0.0104 - 0.011
C_D	5.5113	5.5623	5.57 - 5.59
L_a	0.0840	0.0839	0.0842 - 0.0852
ΔP	0.1158	0.1172	0.1172 - 0.1176

TABLE 3. Test case 2D-1, Re = 20: lift coefficient, drag coefficient, pressure difference between front and rear stagnation points and length of the recirculation zone.

The last two figures show the results obtained for the unsteady case at Reynolds number 100. The contour lines are traced at some large time after the solution has become periodic. In each projection step the maximum absolute value of the divergence was requested to be less than about 10^{-4}. The maximal values of the lift and of the drag coefficients over a period and the Strouhal number are reported, together with the correspondent reference values, in table 4.

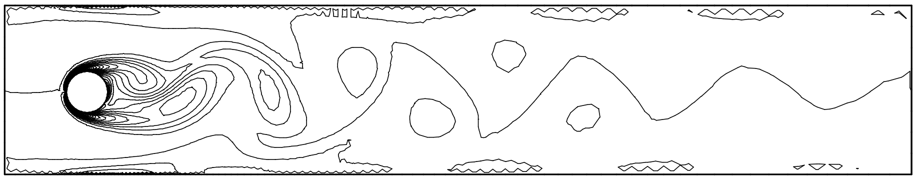

FIGURE 12. Test case 2D-2, Re = 100: vorticity contour lines.

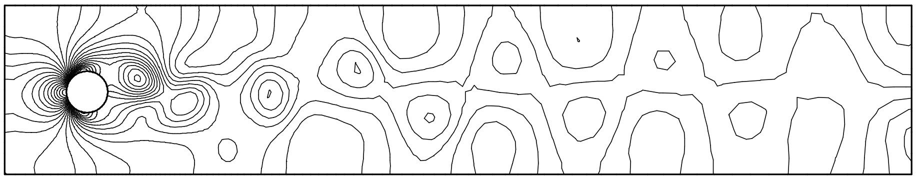

FIGURE 13. Test case 2D-2, Re = 100: pressure contour lines.

	present	reference 1	reference 2
C_{Lmax}	1.002	1.023	0.99 - 1.01
C_{Dmax}	3.200	3.224	3.22 - 3.24
St	0.298	0.297	0.295 - 0.305

TABLE 4. Test case 2D-2, Re = 20: maximum lift coefficient and drag coefficient, Strouhal number.

6. CONCLUSIONS

In this paper we have presented a new finite volume method for the numerical computation of two-dimensional incompressible flows on triangular grids.

The method is second order accurate and can easily deal with complex geometries and with different boundary conditions. Being based on at most piecewise linear ansatz functions and on standard fast iterative Poisson solvers the method is well suited for the extension to the three-dimensional case.

Preliminary results obtained on test problems indicate that the method is both robust and accurate while avoiding local grid decoupling at low Reynolds numbers. Due to the second order Godunov approximation of the convective fluxes the method is well suited for the numerical computation of flows at high Reynolds numbers and for inviscid flows.

Future work will be focused on the following two issues: i) a better understanding of the dependency of the numerical solution on the reconstruction used for the computation of the convective fluxes; ii) the extension of the method to variable density flows.

References

[1] J. Bell A. Almgren and W. Szymczak. A numerical method for the incompressible Navier-Stokes equations based on an approximate projection. *SIAM J. Sci. Comput.*, 17:358–369, 1996.

[2] I. Babuška. The finite element method with Lagrangian multipliers. *Num. Math.*, 20:179–192, 1973.

[3] J. Bell, P. Colella, and H. Glaz. A second-order projection method for the incompressible Navier-Stokes equations. UCRL Preprint 98225, 1988.

[4] J. Bell, P. Colella, and L. Howell. An efficient second-order projection method for the incompressible Navier-Stokes equations on quadrilateral grids. in Proc. 10th AIAA Computational Fluid Dynamics Conference, Honolulu, HI, June 24-27, 1991.

[5] J. Bell and D. Marcus. Vorticity intensification and transition to turbulence in a three-dimensional shear flow. AIAA-91-1649, 22nd AIAA Fluid Dynamics, Plasma Dynamics and Lasers Conference, Honolulu, HI, June 24–27, 1991.

[6] J. Bell and D. Marcus. A Second-Order Projection Method for Variable-Density Flows. *J. Comput. Phys.*, 101:334–348, 1992.

[7] N. Botta and D. Hempel. A finite volume projection method for the numerical solution of the incompressible Navier-Stokes equations on triangular grids. DLR IB 223-96 A 24, 1996.

[8] F. Brezzi. On the existence, uniqueness and approx. of saddle-point problems arising from Lagrange multipliers. *R.A.I.R.O., Anal. Numer. R2*, pages 129–151, 1974.

[9] A. J. Chorin. Numerical Solution of Incompressible Flow Problems. *Studies in Num. Anal.*, 2:64–71, 1968.

[10] A. J. Chorin. Numerical Solution of the Navier-Stokes Equations. *Math. Comp.*, 22:745–762, 1968.

[11] A. J. Chorin. On the convergence of Discrete Approximations to the Navier-Stokes Equations. *Math. Comp.*, 23:341–353, 1968.

[12] O. Friedrich. A new method for generating inner points of triangulations in two dimensions. *Computer Meth. in App. Mech. and Eng.*, 104:77–86, 1993.

[13] P. M. Gresho. Some Interesting Issues in Incompressible Fluid Dynamics, Both in the Continuum and in Numerical Simulation. *Advances in Applied Mechanics*, 28:45–140, 1992.

[14] D. Hempel. Finite Elemente Approximationen für das Stokes-Problem und die Babuška-Brezzi-Bedingung. Master's thesis, Georg-August-Univertität zu Göttingen, 1996.

[15] M. Schäfer and S. Turek. Benchmark computations of laminar flow around a cylinder. Preprint 96-03 (SFB 359) Interdiziplinäres Zentrum für Wissentschaftliches Rechnen der Universität Heidelberg, 1996.

[16] T. E. Tezduyar. Stabilized Finite Element Formulations for Incompressible Flow Computations. *Advances in Applied Mechanics*, 28:1–44, 1992.

[17] K. N. Ghia U. Ghia and C. T. Shin. High-Re Solutions for Incompressible Flow Using the Navier-Stokes equations and a multigrid method. *Journal of Computational Physics*, 48:387–411, 1982.

[18] J. Zhu and J. Sethian. Projection methods coupled to level set interface techniques. *J. Comput. Phys.*, 102:128–138, 1992.

Nicola Botta
Fachbereich Sicherheitstechnik
Bergische Universität, GH
Gauss-str. 20
42097 Wuppertal, Germany.

Daniel Hempel
Institut für Angewandte Mathematik
Universität Hamburg
Bundesstr.55
20146 Hamburg, Germany
e-mail: daniel@math.uni-hamburg.de
fax: ++49 4123 5117